Conductivity percolation of carbon nanotubes (CNT) in polystyrene (PS) latex film

Ş. Uğur, Ö. Yargi, and Ö. Pekcan

Abstract: In this study, the effect of multiwalled carbon nanotubes (MWNT) on film formation behaviour and electrical conductivity properties of polystrene (PS) latex film was investigated by using the photon transmission technique and electrical conductivity measurements. Films were prepared by mixing PS latex with different amounts of MWNTs, varying in the range between 0 and 20 wt%. After drying, MWNT content films were separately annealed above the glass transition temperature (T_g) of PS, ranging from 100 to 270 °C, for 10 min. To monitor film formation behavior of PS–MWNT composites, transmitted light intensity, I_{tr}, was measured after each annealing step. The surface conductivity of annealed films at 170 °C was measured and found to increase dramatically above a certain fraction of MWNT (4 wt%) following the percolation theory. This fraction was defined as the percolation threshold of conductivity, R_c. The conductivity scales with the mass fraction of MWNT as a power law with exponent 2.27, which is extremely close to the value of 2.0 predicted by percolation theory. In addition, the increase in I_{tr} during annealing was explained by void closure and interdiffusion processes. Film formation stages were modeled and the corresponding activation energies were measured.

Key words: multiwalled carbon nanotubes, polystyrene, latex, nanocomposites, conductivity, transmission, percolation, film formation.

Résumé : Faisant appel à la technique de transmission photonique et à des mesures de conductivité électrique, on a étudié l'effet de nanotubes de carbone à parois multiples (NCPM) sur le comportement de formation de films et sur les propriétés de conductivité électrique de films de latex au polystyrène (PS). Les films ont été préparés en mélangeant du latex de PS avec diverses quantités de nanotubes de carbone à parois multiples allant de 0 à 20 % en poids. Après les avoir soumis au séchage, les films contenant des nanotubes de carbone à parois multiples ont été recuits séparément à une température supérieure à la celle de la de transition de verre (T_v) du PS, de 100 à 270 °C, pendant dix minutes. Afin de suivre le comportement de formation des films composites PS/NCPM, on a mesuré l'intensité de la lumière transmise, I_{tr}, après chaque étape de recuisson. On a aussi mesuré la conductivité de surface des films recuits à 170 °C et on a observé une augmentation dramatique au-dessus d'une certaine fraction (4 % en poids), en accord avec la théorie de percolation. On a défini cette fraction comme le seuil de percolation de conductivité, R_c. Les échelles de conductivité utilisant la fraction massique des nanotubes de carbone à parois multiples avec une loi de puissance avec un exposant 2,27 sont très près de la valeur de 2,0 prédite par la théorie de la percolation. De plus, l'augmentation de I_{tr} durant la recuisson peut être expliquée par la fermeture du vide et des processus d'interdiffusion. On a calculé des modèles des stages de formation des films et on a mesuré les énergies d'activation correspondantes.

Mots-clés : nanotubes de carbone à parois multiples, polystyrène, latex, nanocomposites, conductivité, transmission, percolation, formation de film.

[Traduit par la Rédaction]

Introduction

As a result of worldwide efforts by theorists and experimentalists, a very good understanding of the mechanisms of latex film formation has been achieved.[1] Traditionally, the film formation process of polymer latex is considered in terms of three sequential steps: (*i*) Water evaporation and subsequent packing of polymer particles. (*ii*) Deformation of the particles and close contact between the particles if their glass transition temperature (T_g) is less than or close to the drying temperature (soft or low T_g latex). Latex with a T_g above the drying temperature (hard or high T_g latex) stays undeformed at this stage. In the annealing of a hard latex system, deformation of particles first leads to void closure[2–4] and then after the voids disappear, diffusion across particle–particle boundaries starts, i.e., the mechanical properties of hard latex films evolve during annealing, after all solvent has evaporated and all voids have disappeared. (*iii*) Coales-

Received 13 August 2009. Accepted 16 November 2009. Published on the NRC Research Press Web site at canjchem.nrc.ca on 24 February 2010.

This article is part of a Special Issue dedicated to Professor M. A. Winnik.

Ş. Uğur and Ö. Yargi. Department of Physics Istanbul Technical University, Istanbul 34469, Turkey.
Ö. Pekcan.[1] Kadir Has University, Cibali. Istanbul 34230, Turkey.

[1]Corresponding author (e-mail: pekcan@khas.edu.tr).

cence of the deformed particles to form a homogeneous film[3] where macromolecules belonging to different particles mix by interdiffusion.[5,6]

This understanding of latex film formation can now be exploited to underpin the processing of new types of coatings and adhesives. The blending of latex particles and inorganic nanoparticles provides a facile means of ensuring dispersion at the nanometer scale in composite coatings. Carbon nanotubes (CNT) and monodispersed nanoparticles are two of the most important building blocks proposed to create nanodevices. Recently, CNT–polymer nanocomposites have been widely investigated due to their remarkable mechanical,[6] thermal,[7] and electrical properties.[8] CNT have potential applications in many areas such as biosensors, conducting agents, field-effect transistors, and nanocomposites.[9] The polymeric or ceramic matrix of composites is usually considered nonconductive material because of its extremely low electrical conductivity (in the order of 10^{-10}–10^{-15} S/m). Dispersing conductive materials into the nonconductive matrix can form conductive composites. The electrical conductivity of a composite is strongly dependent on the volume fraction of the conductive phase. At low volume fractions, the conductivity remains very close to the conductivity of the pure matrix. When a certain volume fraction is reached, the conductivity of the composite drastically increases by many orders of magnitude. The phenomenon is known as percolation and can be well explained by percolation theory. The electrical percolation threshold of conductive reinforcements embedded in an insulating matrix is sensitive to the geometrical shape of the conductive phase. The small size and large aspect ratio (length/diameter) help lower the percolation threshold.[10] Depending on the matrix, the processing technique, and the nanotube type used, percolation thresholds ranging from 0.001 wt% to more than 10 wt% have been reported.[11,12] Because carbon nanotubes have tremendously large aspect ratios (100–10 000), many researchers have observed exceptionally low electrical percolation thresholds.[12] The electric current-carrying ability of CNTs may be 1000 times that of copper wires.[13] Due to the high aspect ratio of their external shapes, nanotubes can form percolated networks even at very low filler fractions (<5 wt%) to impart tremendous filler reinforcement effects. There have been many studies on low volume fraction composites where the addition of a very small amount of nanotubes substantially modifies the electrical properties of polymer matrices.[13–16] Thus, carbon nanotubes are excellent candidates to blend with polymers to produce electrostatic dissipative materials and other useful components in electronics.

As for the electrical properties of CNT–polymer composites, it was reported that the use of CNTs as conductive fillers in a polymer matrix implies a very low percolation threshold.[13,15,17] However, as CNTs are generally insoluble in common solvents and polymers, they tend to aggregate and disperse poorly in polymer matrix, resulting in deleterious effects. To overcome these difficulties, several methods have been developed to disperse CNTs in host polymers. CNTs could be dispersed in certain polymer solutions via ultrasonication[18–22] or in the presence of surfactants.[23–25] Several groups have reported electrical resistivity results for multiwalled nanotubes (MWNT) and single-walled nanotube (SWNT) ropes.[26] In a recent study ,Gojny et al.[27] concluded that multiwalled carbon nanotubes offer the highest potential for enhancement of electrical conductivity. The rationale behind this conclusion is that the multiwalled nanotubes usually have a better dispersability than single-walled nanotubes. Measured electrical conductivities for nanotube-based composites typically range from 10^{-5} to 10^{-2} S/m for nanotube contents above the percolation threshold.[28] However, electrical conductivity tailored to the range of 0.01–3480 S/m by varying the nanotube content from 0.11 to 15 wt% has also been reported.[17] Surely, the increase of the nanotube volume fraction can increase the electrical conductivity of composites. Previous studies indicate that the overall resistances of SWNT bundle networks and carbon nanotube-based composites are dominated by the contact resistance.[29] Measurements on crossed SWNTs[30] gave contact resistance of 100–400 kΩ for metal–metal or semiconducting–semiconducting SWNT junctions and values two orders higher for metal–semiconducting junctions.

Waviness is a dominant feature of carbon nanotubes in composites. Wavy nanotubes dispersed in a matrix tend to have more contact points than straight nanotubes, and therefore, have a considerable effect on electrical conductivity due to the dominant role of contact resistance. Previous studies have only investigated the effect of waviness on percolation threshold and elastic stiffness of composites.[31–35] The basic conclusion reached in these studies is that the waviness tends to increase the percolation threshold but reduces the elastic stiffness. To date, almost all the computational simulations of the electrical conductivity of nanotube-based composites assumed nanotubes as straight sticks.[34] More recently, Li et al.[36] simulated wavy nanotubes using elongated polygons, and the current carrying backbones of percolation clusters in the composite are identified by a direct electrifying algorithm.[37] The tunneling resistance due to an insulating film of matrix material between crossing nanotubes is considered. Results of Monte Carlo simulations indicate that the electrical conductivity of composites with wavy nanotubes is lower than that of composites with straight nanotubes. In experimental measurements of conductivities, researchers have strived to pursue composite systems with well dispersed fillers. Such an "ideal" system forms a basis for the comparison of conductivity percolation thresholds as influenced by factors such as filler aspect ratio, matrix materials, contact resistance, nanotube waviness, and so forth. The anisotropy of conductivity is strongly affected by nanotube alignment, especially when the nanotube contents are small. But the effect of alignment becomes weaker at larger nanotube contents.[38,39]

In the work reported here, we investigated the film formation behavior and electrical conductivity properties of polymer–CNTs depending on the CNTs content using the photon transmission technique and electrical conductivity measurements. In this work, MWNTs were chosen as conductive fillers rather than single-wall carbon nanotubes (SWNTs) since MWNTs are less expensive than SWNTs and polymer–MWNT composites may be more acceptable than polymer–SWNT composites in industrial application. Furthermore, MWNTs are easier to disperse in the polymer matrix compared to SWNTs. Polystyrene (PS) was used as the polymer matrix because its properties are well-known; it is easy to process, it is soluble in a broad range of solvents, and its

clarity allows dispersion of MWNTs to be optically observed at the micron scale. Films were prepared by mixing PS latex with MWNT particles in various compositions and annealing them at temperatures above the glass transition temperature of PS. After each annealing step, the transmitted light intensity, I_{tr}, was monitored to observe the film formation process. The increase in I_{tr} up to the healing temperature, T_h, and above T_h during annealing was explained by void closure and interdiffusion processes, respectively. From the measurements of the electrical conductivities of the composites, the percolation threshold of conductivity was found to be 4 wt% MWNT.

Experimental

Materials

PS particles were produced via surfactant free emulsion polymerization process. The polymerization was performed batch-wisely using a thermostatted reactor equipped with a condenser, thermocouple, mechanical stirring paddle, and nitrogen inlet. The agitation rate was 400 rpm and the polymerization temperature was controlled at 70 °C. Water (100 mL) and styrene (5 g) were first mixed in the polymerization reactor where the temperature was kept constant (at 70 °C). The potassium peroxodisulfate (KPS) initiator (0.1g), dissolved in small amount of water (2 mL), was then introduced to induce styrene polymerization. The polymerization was conducted during 18 h. The polymer has a high glass transition temperature (T_g = 105 °C). The latex dispersion has an average particle size of 400 nm. Figure 1a shows a scanning electron microscope (SEM) image of the PS latex produced for this study.

Commercially available MWNTs (Cheap Tubes Inc., VT, USA, 10–30 μm long, average inner diameter: 5–10 nm, outer diameter: 20–30 nm, the density is approximately 2.1 g/cm^3, and purity is higher than 95 wt%) were used as supplied in black powder form without further purification. A stock solution of MWNTs was prepared following the manifacturers regulations: nanotubes were dispersed in deionized (DI) water with the aid of polyvinyl pyrolidone (PVP) in the proportions of 10 parts MWNTs, 1–2 parts PVP, 2.000 parts DI water by bath sonication for 3 h. PVP is a good stabilizing agent for dispersions of carbon nanotubes, enabling preparation of polystyrene composites from dispersions of MWNT in polystyrene solution. Figure 1b shows the transmission electron microscope (TEM) image of MWNTs used in this study (www.cheaptubesinc.com).

Preparation of PS–MWNT composite films

A 15 g/L solution of polystyrene (PS) in water was prepared separately. The dispersion of MWNTs in water was mixed with the solution of PS yielding the required ratio, R, of MWNTs in PS latex by using the relation

$$R = \frac{M_{MWNT}}{M_{PS} + M_{MWNT}}$$

where M_{PS} and M_{MWNT} represent the weight of PS and MWNTs in the mixture, respectively. Eighteen different mixtures were prepared with 0, 0.15, 0.45, 0.8, 1, 1.5, 1.8, 2, 2.5, 3, 4, 5, 8, 10, 13, 15, 18, 20 wt% MWNTs by using this relation. Each mixture was stirred for 1 h followed by sonication for 30 min at room temperature. By placing the same number of drops on glass plates with similar surface areas (0.8 × 2.5 cm^2) and allowing the water to evaporate at 60 °C in the oven, dry films were obtained. After drying, samples were separately annealed above the T_g of PS for 10 min at temperatures ranging from 100 to 270 °C. The temperature was maintained within ±2 °C during annealing. After each annealing step, films were removed from the oven and cooled down to room temperature. The thickness of the films was determined from the weight and the density of samples and ranged from 6 to 10 μm.

Fig. 1. (a) SEM image of PS latex and (b) TEM image of multi-walled nanotubes (MWNTs) (www.cheaptubesinc.com) used in this study.

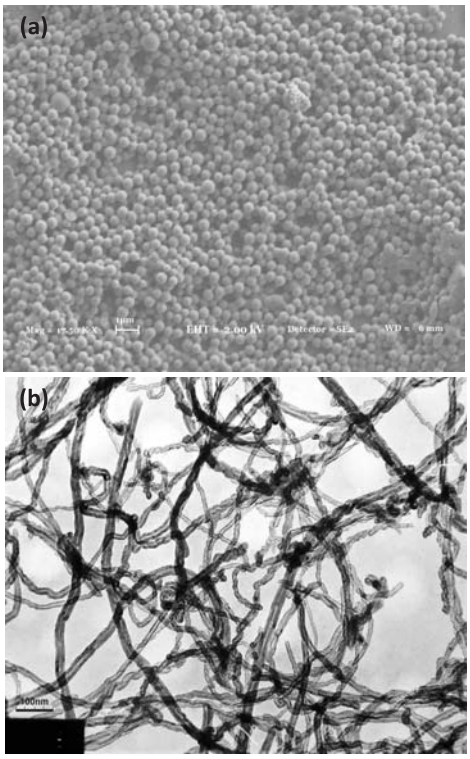

Fig. 2. A schematic illustration of sample position and transmitted light intensity (I_{tr}).

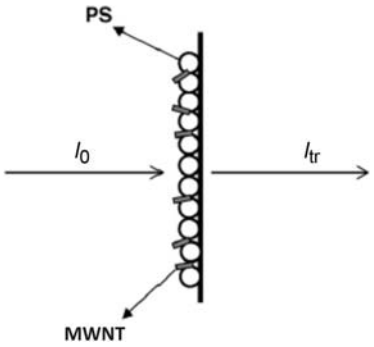

Measurements

Photon transmission experiments were carried out using model Carry 100 bio UV–visible (UVV) spectrometer from Varian. The transmittances of the films were detected at

500 nm at which the composite's spectra is almost flat, i.e., at this wavelength polystyrene and carbon nanotubes have no specific absorption. This picture is quite common for the polymeric films studied using the optical transmission technique.[40–42]. A glass plate was used as a standard for all UVV experiments. The sample position and the transmitted light intensity, I_{tr}, are presented in Fig. 2.

Scanning electron microscope (SEM) images were taken using LEO Supra VP35 FESEM.

Electrical conductivity was measured by a two-probe method using a Keithley Model 6517a Electrometer with an ultrahigh resistance meter. For the surface resistance measurements, the samples were coated onto thin rectangular glass slabs with typical dimensions of 2.0 × 3.0 cm^2. The electrical contact was made using a silver paste. Electrical resistivities of the composite films were measured by alternating polarity technique with electrometer and a test fixture. The composite films were placed in the text fixture, which have disk shaped electrodes, then their surface resistivities, R_s (Ω), were measured for 15 s under 100 V alternating potential. All the resistivities of the composite films were determined for four different orientations and measurements were repeated many times to lower the error level. The surface resistivity was converted into surface conductivity.

Results and discussion

Film formation process of PS–MWNT composites

Transmitted light intensities, I_{tr}, versus annealing temperatures are plotted in Fig. 3 for the films with 0, 1.5, 3, 5, 10, and 15 wt% MWNT content. Upon annealing, the transmitted light intensity, I_{tr}, started to increase for all film samples except for 15 wt% MWNT content film. The increase in I_{tr} with annealing can be explained by the evaluation of the transparency of the films and surface smoothing upon annealing. Most probably, the increase in I_{tr} up to T_h corresponds to the void closure process,[39,43–46] i.e., the polystyrene starts to flow upon annealing and voids between particles can be filled. On the other hand, the increase in I_{tr} above T_h corresponds to the interdiffusion process. However, for 15 wt% MWNT content film, I_{tr} almost doesn't change with annealing, which means that no film formation process occurs, and light transmission is completely blocked by dispersion of the MWNTs in the composite film. On the other hand, I_{tr} decreases with increasing MWNT content in films at all annealing temperatures, predicting that less transparency occurs at high MWNT content films. The plots of the maximum values of $(I_{tr})_{max}$ versus MWNT content in Fig. 4a also confirms this picture, i.e., as the MWNT content is increased, $(I_{tr})_{max}$ first decreases continuously from 70% to 30% at 4 wt% MWNT, and then shows a slight decrease reaching its minimum value (10%) around 15 wt% MWNT.

To see dispersion of MWNTs in PS lattice during annealing, SEM micrographs of composite film with 15 wt% MWNT content were taken after annealing them at 100 and 150 °C (see Fig. 5), respectively. In Fig. 5a, for the 15 wt% MWNT film annealed at 100 °C no deformation in PS particles is observed and PS particles keep their original spherical shapes. After annealing treatment at 150 °C (Fig. 5b), SEM images show that complete particle coalescence has been achieved. It can be clearly seen that the composite film consists of a network of bundles and indicates significant porosity, which results in strong scattering. The optical transmission of the films versus MWNT content above 15 wt% MWNT (Fig. 4a) is a good indicator of how finely nanotubes are dispersed in the matrix. This result is consistent with the microstructural analysis.

The increase in I_{tr} intensity below and above the T_h point in the 0–10 wt% MWNT range can be explained by void closure and interdiffusion processes, respectively.[47] To understand these phenomena, the following mechanisms and their formulations are proposed.

Voids closure

Latex deformation and void closure between particles can be induced by shearing stress, which is generated by surface tension of the polymer, i.e., polymer–air interfacial tension. The void closure kinetics can determine the time for optical transparency and latex film formation.[48] To relate the shrinkage of a spherical void of radius r to the viscosity of the surrounding medium, η, an expression was derived and given by the following relation.[48]

$$[1] \qquad \frac{dr}{dt} = -\frac{\gamma}{2\eta}\left(\frac{1}{\rho(r)}\right)$$

where γ is surface energy, t is time, and $\rho(r)$ is the relative density. It has to be noted here that surface energy causes a decrease in void size and the term $\rho(r)$ varies with the microstructural characteristics of the material, such as the number of voids, the initial particle size, and packing. Equation [1] is similar to one that was used to explain the time dependence of the minimum film formation temperature during latex film formation.[49] If the viscosity is constant in time, the integration of eq. [1] gives the relation as

$$[2] \qquad t = -\frac{2\eta}{\gamma}\int_{r_0}^{r}\rho(r)dr$$

where r_0 is the initial void radius at $t = 0$.

The dependence of the viscosity of the polymer melt on temperature is affected by the overcoming of the forces of macromolecular interaction, which enables the segments of the polymer chain to jump over from one equilibration position to another. This process happens at temperatures at which free volume becomes large enough and is connected with the overcoming of the potential barrier. The Frenkel–Eyring theory produces the following relation for the temperature dependence of viscosity.[50–52]

$$[3] \qquad \eta = (N_0 h/V)\exp(\Delta G/kT)$$

where N_0 is Avagadro's number, h is Planck's constant, V is the molar volume, and k is Boltzmann's constant. It is known that $\Delta G = \Delta H - T\Delta S$, then eq. [3] can be written as

$$[4] \qquad \eta = A\exp(\Delta H/kT)$$

where ΔH is the activation energy of viscous flow, i.e., the amount of heat that must be given to 1 mol of material for creating the act of a jump during viscous flow. ΔS is the entropy of activation of viscous flow. Here, A represents a constant for the related parameters that do not depend on

Fig. 3. Plots of transmitted photon intensities, I_{tr}, vs. annealing temperatures depending on MWNT content in the films. The numbers on each figure show the MWNT content in the film.

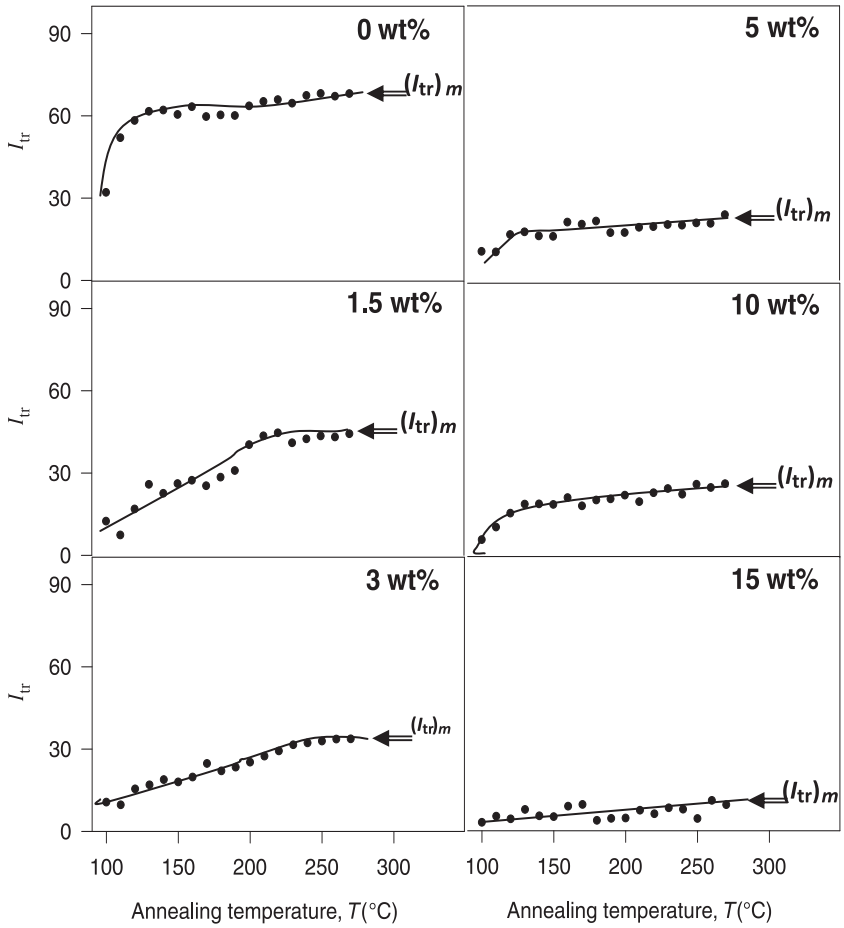

temperature. Combining eq. [2] and [4] the following useful equation is obtained

$$[5] \qquad t = -\frac{2A}{\gamma}\exp\left(\frac{\Delta H}{kT}\right)\int_{r_0}^{r}\rho(r)\mathrm{d}r$$

To quantify the above results, eq. [5] can be employed by assuming that the interparticle voids are equal in size and the number of voids stay constant during film formation (i.e., $\rho(r)\infty r^{-3}$), then integration of eq. [5] gives the relation

$$[6] \qquad t = \frac{2AC}{\gamma}\exp\left(\frac{\Delta H}{kT}\right)\left(\frac{1}{r^2}-\frac{1}{r_0^2}\right)$$

where C is a constant related to the relative density, $\rho(r)$.

To quantify the behavior of I_{tr} curves below T_h presented in Fig. 3, the void closure model can be applied, where a decrease in void size (r) causes an increase in $I_{tr}/(I_{tr})_{max}$ ratios and vice versa. If the assumption is made that the $I_{tr}/(I_{tr})_{max}$ ratio is inversely proportional to the 6th power of the void radius, r, then eq. [6] can be written as

$$[7] \qquad t = \frac{2AC}{\gamma}\exp\left(\frac{\Delta H}{kT}\right)\left(\frac{I_{tr}}{(I_{tr})_{max}}\right)^{1/3}$$

Here, r_0^{-2} is omitted from the relation since it is very small compared to r^{-2} values after a void closure process is started. Equation [7] can be solved for $I_{tr}/(I_{tr})_{max}$

$$[8] \qquad I_{tr}(T) = S(t)\exp\left(\frac{-3\Delta H}{kT}\right)$$

where $S(t) = (yt/2AC)^3$ and $I_{tr} = I_{tr}/(I_{tr})_{max}$. For a given time the logarithmic form of eq. [8] can be written as follows

$$[9] \qquad \ln I_{tr}(T) = \ln S(t) - \left(\frac{3\Delta H}{k_B T}\right)$$

Equation [9] can now be used to produce viscous flow activation energies, ΔH. $\ln I_{tr}$ versus T^{-1} plots and their fits to eq. [9] are presented in Fig. 6 (right hand side of the curves) from which ΔH activation energies were obtained. The measured void closure, ΔH activation energies are listed in Table 1, which are present at a minima around 4 wt%.

Healing and interdiffusion

The decrease in I_{tr} was already explained in the previous section, by the increase in transparency of latex film due to the disappearance of deformed particle–particle interfaces. As the annealing temperature is increased above healing temperature, T_h, some part of the polymer chain may cross the junction surface and particle boundaries start to disappear, as a result, I_{tr} increases due to the shorter optical and

Fig. 4. (a) A plot of the maxima of transmitted light intensities, $(I_{tr})_{max}$, in Fig. 3 vs. MWNT content, R (w/w); (b) log–log plot of $(I_{tr})_{max}$ vs. $(R - R_c)$.

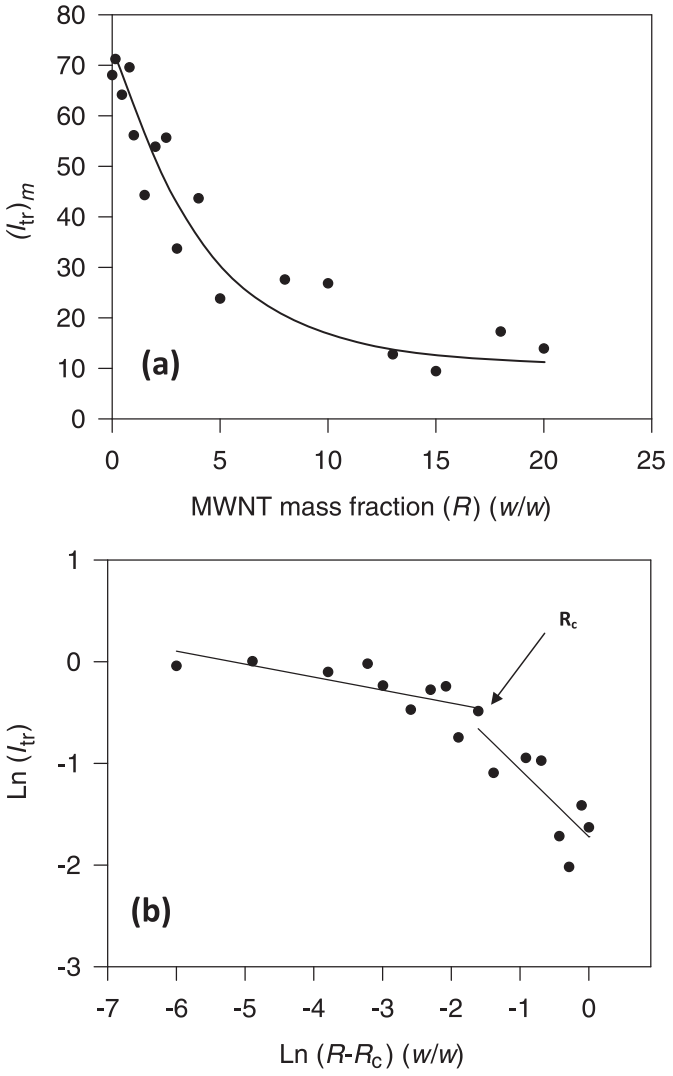

long mean free paths of a photon.[43–47] To quantify these results, the Prager–Tirrell (PT) model[53] for the chain crossing density can be employed. These authors used de Gennes's[54] "reptation" model to explain configurational relaxation at the polymer–polymer junction where each polymer chain is considered to be confined to a tube in which it executes a random back and forth motion. A homopolymer chain with N freely jointed segments of length L was considered by PT, which moves back and forth by one segment with a frequency, ν. In time, the chain displaces down the tube by a number of segments, m. Here, $\nu/2$ is called the "diffusion coefficient" of m in one-dimensional motion. PT calculated the probability of the net displacement with m during time t in the range of $n - \Delta$ to $n - (\Delta + d\Delta)$ segments. A Gaussian probability density was obtained for small times and large N. The total "crossing density", $\sigma(t)$ (chains per unit area), at the junction surface was then calculated from the contributions of $\sigma_1(t)$ due to chains still retaining some portion of their initial tubes, plus a remainder, $\sigma_2(t)$. Here, the $\sigma_2(t)$ contribution comes from chains that have relaxed at least

Fig. 5. SEM images of composite films prepared with 15% MWNT content and annealed for 10 min at (a) 100 and (b) 150 °C temperatures.

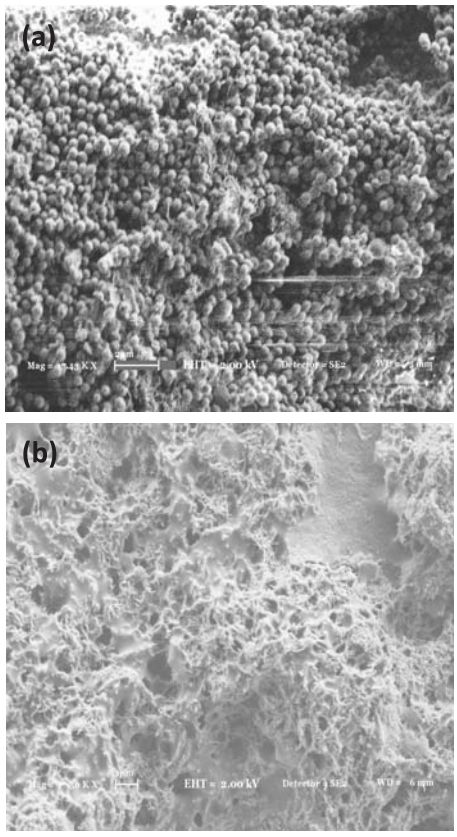

once. In terms of reduced time, $\tau = 2\nu t/N^2$, the total crossing density can be written as

$$[10] \quad \sigma(\tau)/\sigma(\infty) = 2\pi^{-1/2}\left\{\tau^{1/2} + 2\sum_{k=0}^{\infty}(-1)^n[\tau^{1/2}\exp(-k^2/\tau) - \pi^{-1/2}erfc(k/\tau^{1/2})]\right\}$$

For small τ values the summation term of the above equation is very small and can be neglected, which then results in

$$[11] \quad \sigma(\tau)/\sigma(\infty) = 2\pi^{-1/2}\tau^{1/2}$$

This was predicted by de Gennes[54] on the basis of scaling arguments. Here, it should be mentioned that the dependence on time, t, in eq. [10] goes as $t^{1/4}$ at early times of healing.[54,55] To compare our results with the crossing density of the PT model, the temperature dependence of $\sigma(\tau)/\sigma(\infty)$ can be modeled by taking into account the following Arrhenius relation for the linear diffusion coefficient

$$[12] \quad \nu = \nu_o\exp(-\Delta E_b/kT)$$

Here, ΔE_b is defined as the activation energy for backbone motion depending on the temperature interval. Combining eqs. [11] and [12], a useful relation is obtained as

Fig. 6. The $\ln(I_{tr})$ vs. T^{-1} plots of the data in Fig. 3. The slope of the straight lines produces ΔH and ΔE activation energies, which are listed in Table 1.

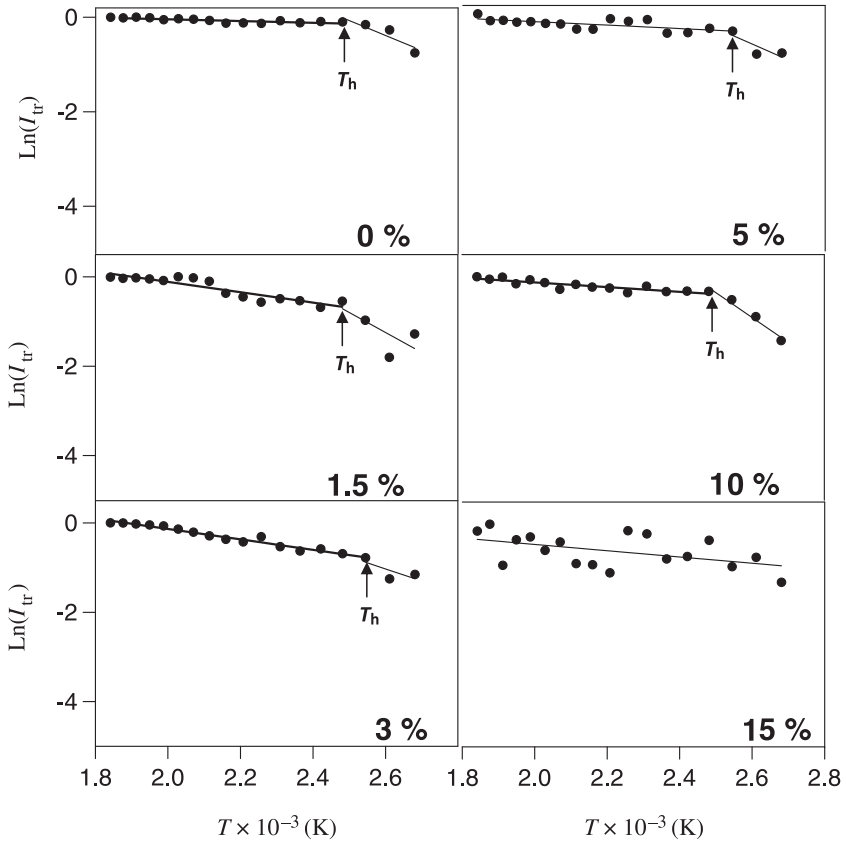

Table 1. Experimentally determined activation energy values.

MWNT (wt%)	0	1.5	2	3	4	5	10	15
ΔH (kcal/mol)	2.1	3.0	1.1	1.8	0.8	2.2	3.7	—
ΔE (kcal/mol)	0.7	4.6	8.6	4.6	5.5	1.4	2.1	—

$$[13] \qquad \sigma(\tau)/\sigma(\infty) = A_o \exp(-\Delta E_b/2kT)$$

where $A_o = (8\nu_o t/\pi N^2)^{1/2}$ is a temperature independent coefficient.

The increase in I_{tr} above T_h is already related to the disappearance of particle–particle interfaces, i.e., as annealing temperature is increased, more chains relax across the junction surface and as a result the crossing density increases. Now, it can be assumed that I_{tr} is proportional to the crossing density, $\sigma(\tau)$, in eq. [13] and then the phenomenological equation can be written as

$$[14] \qquad I_{tr}(T)/I_{tr}(\infty) = A \exp(-\Delta E/2kT)$$

Logarithmic plots of I_{tr} versus T^{-1} are presented in Fig. 6 (left hand side of the curves) for various MWCNT content. The activation energies, ΔE, are produced by least-squares fitting the data to eq. [14] and are listed in Table 1, where it is seen that ΔE values present a maximum around 3 wt% MWNT content, while ΔH values have a minimum about the same point. In other words, the interdiffusion of polymer chains needs more energy to cross over the junction surface than the amount of heat that was required by 1 mol of polymeric material to accomplish a jump during viscous flow. In fact, these optimum points correspond to the percolation threshold for the electrical conductivity and for the optical transparency in composite film (see the next section).

Electrical conductivity of PS–MWNT composites

The surface conductivity properties of the films were measured at room temperature by using a two probe technique. Figure 7a shows the electrical conductivity (σ) of PS–MWNT composite films and its best fit as a function of the MWNTs ratio, R. While low MWNT content composites ($R < 0.04$) show similar conductivity between 10^{-13}–10^{-12} S, the conductivity of high MWNT content films ($R > 0.04$) increase dramatically to $\sim 10^{-7}$–10^{-6} S. In other words, above 0.04 MWNTs form an interconnected percolative network. However, below 0.04, clusters of MWNT become separated by the polystyrene layers. From here we could conclude that the electrical conductivity of the films exhibited a type of percolation[56] behavior since below a certain amount of MWNT, called the percolation threshold, $R_{c\sigma}$ (= 0.04), the conductivity exhibited only a very little change (10^{-13}-10^{-12} S). While for a further increase of MWNTs to above $R_{c\sigma} = 0.04$, the conductivity shows a drastic increase ca. 6–7 orders of magnitude (10^{-7}–10^{-6} S), as compared with low MWNTs content films. Zang and co-workers[57,58] found the percolation threshold is about 4 wt% MWNT for the MWNT–PS composites prepared by the polymerization filling method.

Percolation theory

The basis of the percolation theory is to determine how a

Fig. 7. (a) Conductivity, σ, and its best fitted curve vs. MWNT content, R (w/w); (b) log–log plot of the best fitted curve of σ vs. ($R - R_c$).

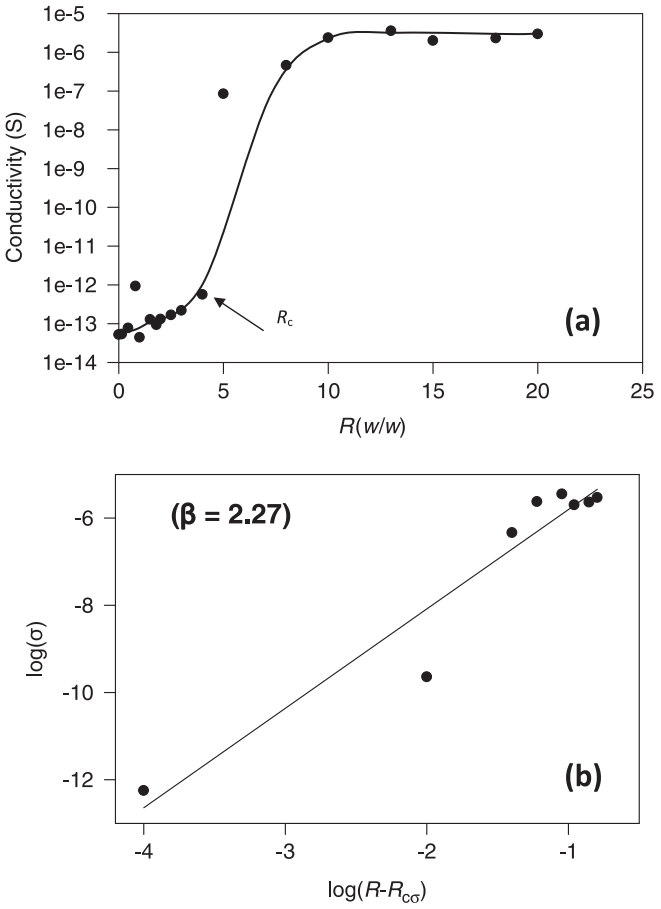

Fig. 8. (a) Scattering light intensity, I_{sc}, and its best fitted curve vs. MWNT content, R (w/w); (b) log–log plot of the best fitted curve of I_{sc} versus ($R - R_c$).

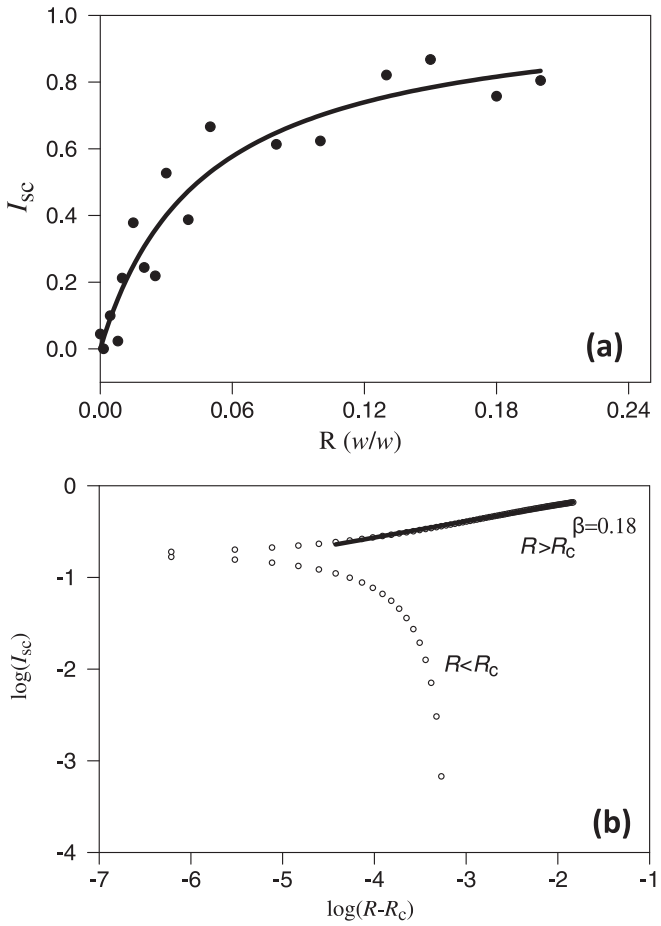

given set of sites, regularly or randomly positioned in some space, is interconnected.[56] At some critical probability, called the "percolation threshold (p_c)", a connected network of sites is formed that spans the sample, causing the system to percolate. In 1957, Broadbent and Hammersley,[59] introduced the term "percolation theory" and used a geometrical and statistical approach to solve the problem of fluid flow through a static medium. Initial work focused on the determination of the percolation thresholds in simple two- and three-dimensional geometries. Two types of percolation were considered: site percolation, where sites in a lattice are either filled or empty, or bond percolation, where all the sites in a lattice are occupied, but are either connected or not.[60] Extensive simulations and theoretical work have shown that the percolation probability, $P_\infty(p)$ vanishes as a power-law near p_c:

$$[15] \qquad p_\infty(p) \approx (p - p_c)^\beta$$

For all volume fractions $p > p_c$, the probability of finding a spanning cluster extending from one side of the system to the other side is 1. The largest cluster spans the lattice connecting the left and right edges to the bottom edge, which is called "percolating cluster". Whereas for all volume fractions $p < p_c$, the probability of finding such an infinite cluster is 0.

The concept of percolation has been applied to many diverse applications, including the spread of disease in a population, flow through a porous medium, quarks in nuclear matter, and variable range hopping in amorphous semiconductors.[61] Percolation theory has been used to interpret the behaviour in a mixture of conducting and nonconducting components.[62] The sudden transition in such materials from insulator to conductor is evidence of a percolation threshold. The conductivity, σ, of a percolative system is generally described as a function of the mass fraction, R, by the scaling law in the vicinity of the percolation threshold ($R_{c\sigma}$):

$$[16] \qquad \sigma = \sigma_0(R - R_{c\sigma})^{\beta_\sigma}$$

where σ is the composite conductivity (in Siemens), σ_0 is the self conductivity of MWNTs film and is equal to 1. R represents the weight fraction of MWNTs, $R_{c\sigma}$ represents the percolation threshold of conductivity, and β_σ is the critical exponent. This equation is valid at concentrations above the percolation threshold, i.e., when $R > R_{c\sigma}$. The value of the critical exponents, β_σ, is dependent on the dimensions of the lattice.[59]

To calculate the percolation threshold, eq. [16] was transformed into the logarithmic form:

$$[17] \qquad \log(\sigma) = \log(\sigma_0) + \beta_\sigma \log|R - R_c|$$

Then to produce an estimated value for $R_{c\sigma}$ and the critical exponent β_σ we fitted the $\log(\sigma) - \log|R - R_c|$ data in Fig. 7b for $R > R_{c\sigma}$, to eq. [17]. Here, due to the limitation on getting more data in critical region, we used the continuous function fitted best to the experimental points in Fig. 7a. The goodness of the fit was around $r^2 \approx 0.9$. The value of β_σ has been determined from the slope of the linear relation of $\log(\sigma) - \log|R - R_c|$ plot of the best fitted curve in Fig. 7b and found to be 2.27. This value agrees well with the universal scaling value of $\beta_\sigma = 2.0$. The difference between the theoretical and experimental values (13.5%) might be explained with the errors originating from the fitting. In three-dimensional lattice systems[60] β_σ values change from 1.3 to 3. The fact that β_σ is not significantly greater than 2.0 also suggests that the bundles are not separated by polymer tunneling barriers and shows that the polymer coating observed in Fig. 5 cannot simply coat individual bundles but must coat the network as a whole, allowing intimate contact between bundles at junction sites.

On the other hand, as seen in Fig. 4*a*, the inclusion of MWNTs into the PS lattice strongly decreases the transmitted light intensity. This finding can be rationalized by first assuming that σ is proportional to the scattered light intensity, $I_{sc} = 1 - (I_{tr})_{max}$, by obeying the following relation

$$[18] \qquad I_{sc}(R) = (R - R_c)^\beta$$

Here, it should be realized that inclusions of MWNTs into the PS lattice creates a two phase heterogeneous structure, which causes light scattering from the composite film surface, while the conductivity increases in the same fashion. Equation [18] describes the percolation model for MWNTs distribution in the PS lattice where R_c was produced in Fig. 4b from the intersection of two broken straight lines. When R approaches R_c, the largest cluster of MWNTs appears by connecting the left and right edges to the bottom edge of the MWNTs.

The scattered light intensity, I_{sc}, versus MWNTs content and its best fit are plotted in Fig. 8a, where it is seen that I_{sc} has increased to large values for all samples above 4 wt% MWNT content. This behavior of scattering light intensity can be explained by percolating MWNT particles in the PS lattice. In Fig. 8b, the log–log plot of eq. [18] is fitted to the data in Fig. 8a, where the slope of the straight line produced the critical exponent, $\beta = 0.18$, above $R_c = 0.04$, which is not so far from the bond-percolation theory. In a simple cubic lattice β is found to be 0.25 for the bond percolation model.[56]

Conclusions

We have reported an investigation of the film formation and electrical conductivity of PS–MWNT composites. Below 10 wt% MWNT content, two distinct film formation stages, which are named as void closure and interdiffusion, were observed. However, MWNT concentrations above 10 wt% MWNT, no film formation can be achieved. On the other hand, sample conductivities were observed to depend strongly on the MWNT contents, which are drastically changed with an increase of the MWNT content above the percolation threshold of 4 wt% MWNT. With the introduction of 4 wt% MWNTs, the conductivity presented an increase by 6–7 orders of magnitude compared with low MWNT content films.

Void closure (ΔH) and interdiffusion (ΔE) activation energies presented optimum values around the threshold of the electrical contuctivity and optical transparency percolation around 4 wt% MWNT content. Our results are quite similar to other reports on low conductance with CNTs amounts and start to saturate at higher CNTs content. Further investigation of electrical properties of the composite films is underway in our laboratory to understand the behaviors of (ΔH) and (ΔE) activation energies around the percolation point.

Acknowledgement

Professor Pekcan would like to thank the Turkish Academy of Sciences for their partial support.

References

(1) *Film Formation in Waterborne Coatings;* Provder, T., Winnik, M. A., Urban, M. W., Eds., ACS Symposium Series 648; American Chemical Society: Washington, DC, 1996.
(2) Sperry, P. R.; Snyder, B. S.; O'Dowd, M. L.; Lesko, P. M. *Langmuir* **1994**, *10* (8), 2619. doi:10.1021/la00020a021.
(3) Mackenzie, J. K.; Shuttleworth, R. *Proc. Phys. Soc.* **1949**, *62B*, 833. doi:10.1088/0370-1301/62/12/310.
(4) Keddie, J. L. *Mater. Sci. Eng.* **1997**, *R21*, 101.
(5) Yoo, J. N.; Sperling, L. H.; Glinka, C. J.; Klein, A. *Macromolecules* **1991**, *24* (10), 2868. doi:10.1021/ma00010a036.
(6) Pekcan, Ö. *Trends Polym. Sci.* **1994**, *2*, 236.
(7) Baughman, R. H.; Zakhidov, A. A.; de Heer, W. A. *Science* **2002**, *297* (5582), 787. doi:10.1126/science.1060928. PMID: 12161643.
(8) Coleman, J. N.; Khan, U.; Blau, W. J.; Gun'ko, Y. K. *Carbon* **2006**, *44* (9), 1624. doi:10.1016/j.carbon.2006.02.038.
(9) Ajayan, P. M.; Zhou, O. Z. *Top. Appl. Phys.* **2001**, *80*, 391. doi:10.1007/3-540-39947-X_14.
(10) Bigg, D. M.; Stutz, D. E. *Polym. Compos*. **1983**, *4* (1), 40. doi:10.1002/pc.750040107.
(11) Grunlan, J. C.; Mehrabi, A. R.; Bannon, M. V.; Bahr, J. L. *Adv. Mater.* **2004**, *16* (2), 150. doi:10.1002/adma.200305409.
(12) Kymakis, E.; Alexandou, I.; Amaratunga, G. A. J. *Synth. Met.* **2002**, *127* (1–3), 59. doi:10.1016/S0379-6779(01)00592-6.
(13) Sandler, J. K. W.; Kirk, J. E.; Kinloch, I. A.; Shaffer, M. S. P.; Windle, A. H. *Polymer (Guildf.)* **2003**, *44* (19), 5893. doi:10.1016/S0032-3861(03)00539-1.
(14) Bin, Y.; Kitanaka, M.; Zhu, D.; Matsuo, M. *Macromolecules* **2003**, *36* (16), 6213. doi:10.1021/ma0301956.
(15) Sandler, J.; Shaffer, M. S. P.; Prasse, T.; Bauhofer, W.; Schulte, K.; Windle, A. H. *Polymer (Guildf.)* **1999**, *40* (21), 5967. doi:10.1016/S0032-3861(99)00166-4.
(16) Murphy, R.; Nicolosi, V.; Hernandez, Y.; McCarthy, D.; Rickard, D.; Vrbanic, D.; Mrzel, A.; Mihailovic, D.; Blau, W. J.; Coleman, J. N. *Scr. Mater.* **2006**, *54* (3), 417. doi:10.1016/j.scriptamat.2005.10.015.
(17) Ramasubramaniam, R.; Chen, J.; Liu, H. Y. *Appl. Phys. Lett.* **2003**, *83* (14), 2928. doi:10.1063/1.1616976.
(18) Barrau, S.; Demont, P.; Peigney, A.; Laurent, C.; Lacabanne, C. *Macromolecules* **2003**, *36* (14), 5187. doi:10.1021/ma021263b.
(19) Ruan, S. L.; Gao, P.; Yang, X. G.; Yu, T. X. *Polymer (Guildf.)* **2003**, *44* (19), 5643. doi:10.1016/S0032-3861(03)00628-1.

(20) Geng, H.; Rosen, R.; Zheng, B.; Shimoda, H.; Fleming, L.; Liu, J.; Zhou, O. *Adv. Mater.* **2002**, *14* (19), 1387. doi:10.1002/1521-4095(20021002)14:19<1387::AID-ADMA1387>3.0.CO;2-Q.
(21) Jin, L.; Bower, C.; Zhou, O. *Appl. Phys. Lett.* **1998**, *73* (9), 1197. doi:10.1063/1.122125.
(22) Qian, D.; Dickey, E. C.; Andrews, R.; Rantell, T. *Appl. Phys. Lett.* **2000**, *76* (20), 2868. doi:10.1063/1.126500.
(23) Tang, B. Z.; Xu, H. *Macromolecules* **1999**, *32* (8), 2569. doi:10.1021/ma981825k.
(24) Barrau, S.; Demont, P.; Perez, E.; Peigney, A.; Laurent, C.; Lacabanne, C. *Macromolecules* **2003**, *36* (26), 9678. doi:10.1021/ma030399m.
(25) Jin, Z.; Huang, L.; Goh, S. H.; Xu, G.; Ji, W. *Chem. Phys. Lett.* **2000**, *332* (5–6), 461. doi:10.1016/S0009-2614(00)01294-X.
(26) Schadler, L. S.; Giannaris, S. C.; Ajayan, P. M. *Appl. Phys. Lett.* **1998**, *73* (26), 3842. doi:10.1063/1.122911.
(27) Gojny, F. H.; Wichmann, M. H. G.; Fiedler, B.; Kinloch, I. A.; Bauhofer, W.; Windle, A. H.; Schulte, K. *Polymer (Guildf.)* **2006**, *47* (6), 2036. doi:10.1016/j.polymer.2006.01.029.
(28) McNally, T.; Pötschke, P.; Halley, P.; Murphy, M.; Martin, D.; Bell, S. E. J.; Brennan, G. P.; Bein, D.; Lemoine, P.; Quinn, J. P. *Polymer (Guildf.)* **2005**, *46* (19), 8222. doi:10.1016/j.polymer.2005.06.094.
(29) Stadermann, M.; Papadakis, S. J.; Falvo, M. R.; Novak, J.; Snow, E.; Fu, Q.; Liu, J.; Fridman, Y.; Boland, J.; Superfine, R.; Washburn, S. *Phys. Rev. B* **2004**, *69* (20), 201402R. doi:10.1103/PhysRevB.69.201402.
(30) Fuhrer, M. S.; Nygard, J.; Shih, L.; Forero, M.; Yoon, Y. G.; Mazzoni, M. S. C.; Choi, H. J.; Ihm, J.; Louie, S. G.; Zettl, A.; McEuen, P. L. *Science* **2000**, *288* (5465), 494. doi:10.1126/science.288.5465.494. PMID:10775104.
(31) Yi, Y. B.; Berhan, L.; Sastry, A. M. *J. Appl. Phys.* **2004**, *96* (3), 1318. doi:10.1063/1.1763240.
(32) Berhan, L.; Sastry, A. M. *Phys. Rev. E: Stat. Nonlinear Soft Matter Phys.* **2007**, *75* (4), 041121. PMID:17500879.
(33) Fisher, F. T.; Bradshaw, R. D.; Brinson, L. C. *Compos. Sci. Technol.* **2003**, *63* (11), 1689. doi:10.1016/S0266-3538(03)00069-1.
(34) Shi, D. L.; Feng, X. Q.; Huang, Y. G. Y.; Hwang, K. C.; Gao, H. J. *J. Eng. Mater. Technol.* **2004**, *126* (3), 250. doi:10.1115/1.1751182.
(35) Wu, S.-H.; Masaharu, I.; Natsuki, T.; Ni, Q.-Q. *J. Reinf. Plast. Compos.* **2006**, *25* (18), 1957. doi:10.1177/0731684406069923.
(36) Li, C. Y.; Thostenson, E. T.; Chou, T. W. *Compos. Sci. Technol.* **2008**, *68* (6), 1445. doi:10.1016/j.compscitech.2007.10.056.
(37) Li, C. Y.; Chou, T. W. *J. Phys A: Math. Theor.* **2007**, *40*, 14679. doi:10.1088/1751-8113/40/49/004.
(38) Du, F. M.; Fischer, J. E.; Winey, K. I. *J. Polym. Sci., Part B: Polym. Phys.* **2003**, *41* (24), 3333. doi:10.1002/polb.10701.
(39) Du, F. M.; Fischer, J. E.; Winey, K. I. *Phys. Rev. B* **2005**, *72* (12), 121404. doi:10.1103/PhysRevB.72.121404.
(40) Arda E, Bulmus V, Piskin E. *J. Colloid Interface Sci.* **1999**, *213* (1), 160. doi:10.1006/jcis.1998.6051.
(41) Arda, E.; Pekcan, Ö. *Polymer (Guildf.)* **2001**, *42* (17), 7419. doi:10.1016/S0032-3861(01)00131-8.
(42) Pekcan, Ö.; Arda, E.; Kesenci, K.; Pişkin, E. *J. Appl. Polym. Sci.* **2001**, *79*, 2014. doi:10.1002/1097-4628(20010314)79:11<2014::AID-APP1010>3.0.CO;2-3.
(43) Pekcan, Ö.; Arda, E. *Encyclopedia of Surface and Colloid Science;* Marcel and Dekker: New York, 2002; p 2691.
(44) Pekcan, Ö.; Arda, E.; Bulmuş, V.; Pişkin, E. *J Appl. Polym. Sci.* **2000**, *77* (4), 866. doi:10.1002/(SICI)1097-4628(20000725)77:4<866::AID-APP21>3.0.CO;2-9.
(45) Arda, E.; Özer, F.; Pişkin, E.; Pekcan, Ö. *J. Colloid Interface Sci.* **2001**, *233* (2), 271. doi:10.1006/jcis.2000.7234. PMID:11121276.
(46) Arda, E.; Pekcan, Ö. *Polymer (Guildf.)* **2001**, *42* (17), 7419. doi:10.1016/S0032-3861(01)00131-8.
(47) Uður, S.; Yargi, Ö.; Pekcan, Ö. *Compos. Interfaces* **2008**, *15* (4), 411. doi:10.1163/156855408784514748.
(48) Keddie, J. L.; Meredith, P.; Jones, R. A. L.; Donald, A. M. *Film Formation in Waterborne Coatings;* Provder, T., Winnik, M. A., Urban, M.W., Eds.; ACS Sympymposium Series 648; American Chemical Society: Washington, DC, 1996; pp 332–348.
(49) Mc Kenna, G. B. In *Comprehensive Polymer Science;* Booth, C., Price C., Eds.; Pergamon Press: Oxford, UK, 1989; p 2.
(50) Vogel, H. *Phys. Z.* **1925**, *22*, 645.
(51) Fulcher, G. S. *J. Am. Ceram. Soc.* **1925**, *8* (6), 339. doi:10.1111/j.1151-2916.1925.tb16731.x.
(52) Frenkel, J. *J. Phys. USSR* **1945**, *9*, 385.
(53) (a) Prager, S.; Tirrell, M. *J. Chem. Phys.* **1981**, *75* (10), 5194. doi:10.1063/1.441871.; (b) Wool, R. P.; Yuan, B.-L.; McGarel, O. J. *Polym. Eng. Sci.* **1989**, *29* (19), 1340. doi:10.1002/pen.760291906.
(54) de Gennes, P. G. *J. Chem. Phys.* **1982**, *76* (6), 3322. doi:10.1063/1.443329.
(55) (a) Kim, Y. H.; Wool, R. P. *Macromolecules* **1983**, *16* (7), 1115. doi:10.1021/ma00241a013.; (b) Wool, R. P.; O'Connor, K. M. *J. Appl. Phys.* **1981**, *52* (10), 5953. doi:10.1063/1.328526.
(56) Stauffer, D.; Aharony, A. *Introduction to Percolation Theory;* Taylor & Francis: London, 1994.
(57) Dong, X. M.; Fu, R. W.; Zhang, M. Q.; Zhang, B.; Li, J. R.; Rong, M. Z. *Carbon* **2003**, *41* (2), 371. doi:10.1016/S0008-6223(02)00336-6.
(58) Zhang, B.; Fu, R. W.; Zhang, M. Q.; Dong, X. M.; Lan, P. L.; Qiu, J. S. *Sens. Actuators, B* **2005**, *109* (2), 323. doi:10.1016/j.snb.2004.12.066.
(59) Broadbent, S. R.; Hammersley, J. M. *Proc. Camb. Philos. Soc.* **1957**, *53* (03), 629. doi:10.1017/S0305004100032680.
(60) Sahimi, M. Applications of Percolation Theory London: Taylor and Francis (1994).
(61) Lux, F. *J. Mater. Sci.* **1993**, *28* (2), 285. doi:10.1007/BF00357799.
(62) Kirkpatrick, S. *Rev. Mod. Phys.* **1973**, *45* (4), 574. doi:10.1103/RevModPhys.45.574.